Contents lists available at ScienceDirect

Arabian Journal of Chemistry

journal homepage: www.ksu.edu.sa

Original article

Pyrimidine derivatives as efficient anticorrosive agents for acid corrosion of mild steel: Electrochemical and computational validation

Aeshah H. Alamri [a,*], Kedila Rasheeda [b], Salwa J. Kamal [a], Marwah Aljohani [a], Talal A. Aljohani [c], Irshad Baig [d], Vijaya D.P. Alva [b], N. Phadke Swathi [e], Ikenna B. Onyeachu [f], Seranthimata Samshuddin [g,h,*]

[a] Chemistry Department, College of Science, Imam Abdulrahman Bin Faisal University, P.O. Box 76971, Dammam 31441, Saudi Arabia
[b] Department of Chemistry, Shree Devi Institute of Technology, Kenjar, Mangalore 574142 and affiliated to Visvesvaraya Technological University, Belagavi, Karnataka, India
[c] Refining Technologies and Petrochemicals Institute, King Abdulaziz City for Science and Technology (KACST), Riyadh 12354, Saudi Arabia
[d] Basic & Applied Scientific Research Center, Imam Abdulrahman Bin Faisal University, P.O. Box 1982, Dammam 31441, Saudi Arabia
[e] Department of Chemistry, Sri Dharmasthala Manjunatheshwara Institute of Technology, Ujire 574240 and affiliated to Visvesvaraya Technological University, Belagavi, Karnataka, India
[f] Department of Chemistry, Edo State University Uzairue, P.M.B. 04 Auchi, Edo State, Nigeria
[g] Department of Chemistry, Alva's Institute of Engineering and Technology, Mijar, Moodubidire 574225 and affiliated to Visvesvaraya Technological University, Belagavi, Karnataka, India
[h] Department of PG Studies in Chemistry, Alva's College (Autonomous), Vidyagiri, Moodubidire 574227 Karnataka, India

ARTICLE INFO

Keywords:
Corrosion inhibitor
Mild steel
Pyrimidine derivatives
SEM
DFT
Langmuir adsorption

ABSTRACT

The present study aims to assess the potential of three pyrimidine derivatives—namely, ethyl 4-[4-(dimethylamino)phenyl]-2-imino-6-methyl-1,2,3,4-tetrahydropyrimidine-5-carboxylate (EDTP), 1-{4-[4-(dimethylamino) phenyl]-2-imino-6-methyl-1,2,3,4-tetrahydropyrimidin-5-yl}ethan-1-one (DITP), and 4-[4-(dimethylamino) phenyl]-2-imino-6-methyl-*N*-phenyl-1,2,3,4-tetrahydropyrimidine-5-carboxamide (DPTP)—in protecting mild steel against acidic corrosion. The anti-corrosive effectiveness of these synthesized pyrimidine derivatives is evaluated using various electrochemical techniques. Based on the electrochemical findings, it is observed that all synthesized pyrimidine derivatives function as mixed-type inhibitors. Notably, DPTP demonstrates superior efficacy at 750 ppm (91.7 %) in comparison to EDTP (88.9 %) and DITP (88.4 %). Analysis utilizing the Langmuir isotherm model reveals the most precise correspondence with the studied derivatives, suggesting a mixed mode of adsorption involving both chemisorption and physisorption. Furthermore, a surface analysis investigation is conducted to assess the morphology of metallic surfaces exposed to varying inhibitor concentrations within an acidic environment. To corroborate the experimental findings, theoretical approaches including Monte Carlo simulation (MC simulation) and density functional theory (DFT) have been employed.

1. Introduction

Corrosion significantly alters the material properties of metals, notably impacting their strength and longevity. Literature suggests that around 34 % of the global Gross Domestic Product (GDP) is spent annually to mitigate the adverse economic effects of corrosion (Koch, 2017; Ferigita et al., 2023). Steel, renowned for its widespread usage across various industries, owes its popularity to attributes such as affordability, availability, hardness, malleability, flexibility, ductility, high tensile strength, and a high melting point (Paul and Yadav, 2020).

The susceptibility of steel to corrosion, particularly when exposed to dilute mineral acids, remains a persistent issue in industrial settings. This susceptibility leads to active corrosion on the steel surface, impeding the formation of a protective layer against corrosion. This vulnerability is notably evident during industrial acid cleaning processes aimed at removing inorganic scales that accumulate and disrupt efficiency during application (Yüce et al., 2014). Hydrochloric acid is commonly employed for acid cleaning due to its effectiveness in converting inorganic scales into soluble chlorides (Yadav et al., 2015a; Yadav et al., 2015b; Yadav, Sharma, and Yadav, 2013; Assad et al.,

* Corresponding authors.
E-mail addresses: ahalamri@iau.edu.sa (A.H. Alamri), samshu486@gmail.com (S. Samshuddin).

https://doi.org/10.1016/j.arabjc.2024.105752
Received 3 December 2023; Accepted 21 March 2024
Available online 4 April 2024

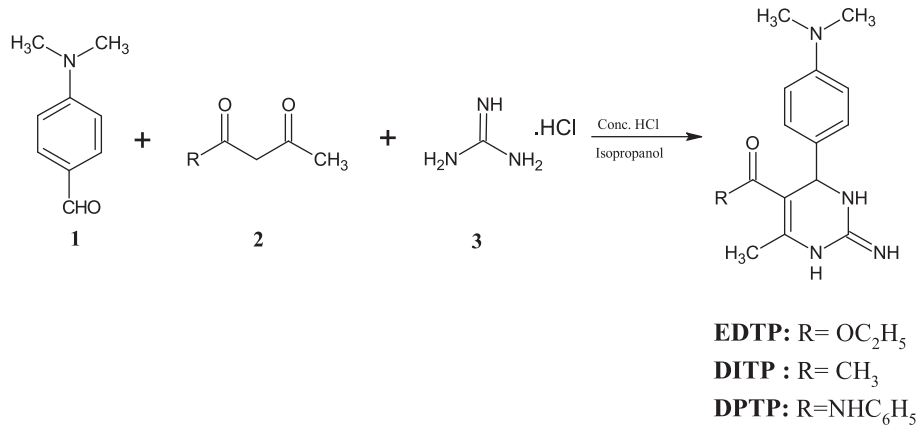

Scheme 1. Synthesis of EDTP, DITP and DPTP.

2023; Verma, Quraishi, and Singh, 2015). However, the simultaneous corrosion attack on the underlying steel raises significant industrial concerns, necessitating effective corrosion mitigation strategies.

One such approach involves the use of chemical substances known as corrosion inhibitors, which offer efficient, cost-effective, sustainable, and industrially scalable solutions for protecting steel surfaces from acid corrosion (Verma et al., 2021; Obot, Onyeachu, and Umoren, 2018; Ouakki, Galai, and Cherkaoui, 2022; Avdeev and Kuznetsov, 2021). These inhibitors are expected to safeguard the steel surface with high efficiency at minimal cost when applied in low doses (Chauhan, Qurashi, and Qurashi, 2021; Obot et al., 2019a).

Pyrimidine derivatives have emerged as potential candidates for developing highly efficient acid corrosion inhibitors due to their unique properties. Characterized by a heterocyclic six-membered structure with nitrogen atoms at positions 1 and 3, pyrimidine possesses characteristics that enable effective engagement in donor–acceptor interactions with metals (Onyeachu, Quraishi, and Obot, 2023a; Onyeachu et al., 2019; Verma et al., 2023). However, there is a lack of reports detailing the effect of substituent groups on the corrosion inhibition performance of pyrimidine derivatives, essential for the design and development of commercial acid corrosion inhibitors.

In view of the importance of pyrimidine derivatives, it was decided to synthesize three pyrimidine derivatives with different substituent groups (EDTP, DITP, and DPTP). These compounds stand out due to their innovative features, which include a green synthesis approach through one-step multicomponent synthesis. This method not only minimizes environmental impact but also streamlines production, making it economically feasible for large-scale applications. Their optimized solubility in acidic environments may ensure effective dispersion and coverage on steel surfaces, enhancing their protective capabilities. Additionally, the molecular structure of these pyrimidine derivatives provides an abundance of adsorption sites, which may facilitate strong interactions with metal surfaces and the formation of a durable protective layer against corrosion. Subsequently, the impact of these pyrimidine derivatives on the mechanism of steel corrosion in a 1.0 M HCl acid solution has been evaluated using electrochemical methods including Open circuit potential (OCP), Linear polarization resistance (LPR), Potentiodynamic polarization (PDP), Electrochemical impedance spectroscopy (EIS), and Electrochemical frequency modulation (EFM). Additionally, the effect of EDTP, DITP, and DPTP on the damage to the steel surface microstructure was investigated using scanning electron microscopy (SEM) and energy dispersive X-ray analysis (EDX). Computational calculations based on density functional theory (DFT) and Monte Carlo simulation provided molecular-level insights into the inhibitor-steel interaction.

Table 1
Characterization data of EDTP, DITP and DPTP

Characterization Technique	EDTP	DITP	DPTP
Melting point	172-175^{0}C	185-188^{0}C	191-193^{0}C
^{1}H NMR (400 MHz, δ ppm)	1.15 (t, 3H, *J* = 14 Hz, Ethyl-CH_3), 2.21 (s, 3H, Pyrimidine CH_3), 2.80 (s, 6H, NCH_3), 3.91 (q, 2H, CH_2, *J* = 14 Hz,), 5.08 (s, 1H, Pyrimidine ring CH), 6.61 (d, 2H, *J* = 18 Hz, Ar-H), 6.99 (d, 2H, *J* = 18 Hz, Ar-H), 7.66 (s, 1H, NH), 9.04 (s, 1H, NH)	1.98 (s, 3H, $COCH_3$), 2.22 (s, 3H, Pyrimidine-CH_3), 2.82 (s, 6H, NCH_3), 4.96 (s, 1H, Pyrimidine ring CH), 6.59 (d, 2H, *J* = 18 Hz, Ar-H), 6.98 (d, 2H, *J* = 18 Hz, Ar-H), 7.58 (s, 1H, NH), 9.09 (s, 1H, NH)	2.01 (s, 3H, Pyrimidine-CH_3), 2.78 (s, 6H, NCH_3), 5.11 (s, 1H, Pyrimidine ring CH), 6.76 (d, 2H, *J* = 18 Hz, Ar-H), 7.17 (d, 2H, *J* = 18 Hz, Ar-H), 7.42 (m, 3H, Ar-H), 7.50 (d, 2H, Ar-H) 8.50 (s, 1H, NH), 9.46 (s, 1H, NH)
IR (cm^{-1})	3408 (pyrimidine NH), 3043 (aromatic CH), 2924 (aliphatic CH), 1724 (C=O), 1595 (C=N)	3452 (pyrimidine NH), 3064 (aromatic CH), 2900 (aliphatic CH), 1681 (C=O), 1598 (C=N)	3313 (pyrimidine NH), 2937 (aliphatic CH), 1654 (C=O), 1593 (C=N)

2. Methods and materials

2.1. Synthesis procedure of inhibitors (EDTP, DITP, and DPTP)

All three pyrimidine derivatives were synthesized using an eminent Biginelli reaction, as depicted in Scheme 1 (Bigi et al., 1999). The precursor, *p*-dimethyl aminobenzaldehyde **1** (0.01 mol), was made soluble in isopropanol and taken in a RB flask. The solution was mixed with ethyl acetoacetate **or** acetyl acetone **or** aceto aetanilide **2** (0.015 mol), guanidine hydrochloride **3** (0.01 mol), and a drop of conc. HCl. The resultant solution was refluxed about 80ºC for 12 h. After the complete conversion of reactants to the product, the resulting solution was refrigerated and the resultant solid obtained after filtration was dried and crystallized from dimethyl formamide. The yield of EDTP, DITP, and DPTP was found to be 83 %, 86 %, and 81 %, respectively. The spectral data of EDTP, DITP, and DPTP are presented in Table 1.

2.2. Electrochemical tests

In the current corrosion investigation, 1.0 M HCl was the medium. Mild steel was utilized for the electrochemical examinations, and its surface area was 5.23 cm^2. Electrochemical measurements were achieved using interface 1010 E Potentiostat operated by Gamry

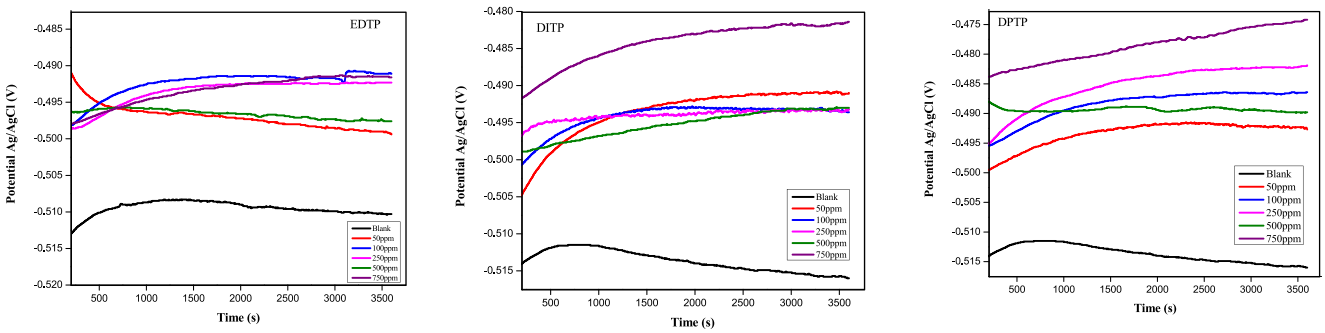

Fig. 1. Open circuit potential plots for the corrosion inhibition of mild steel in 1.0 M HCl at 298 K without and with various concentrations of EDTP, DITP and DPTP.

Instruments, U.S.A. as described in our previous paper (Rasheeda et al., 2022a, 2022b; Swathi,et al., 2023).

2.3. Surface examination

After immersing steel samples in both inhibited and uninhibited 1.0 M HCl for 12 h, surface morphology characterization was achieved using the SEM model JSM–7100F which was hyphenated to an EDX detector ESCALAB 250Xi (Thermo Fisher Scientific, USA) for analyzing chemical composition of the corrosive product (Fytianos et al., 2016).

2.4. DFT study

Quantum chemical parameters of the inhibitors were determined with the aid of Materials Studio 7.0 commercial software (Accelrys Inc. U.S.A.) and COMPASS force field (Sun, 1998). The frontier orbitals were calculated in the gaseous phase via DMol^3 module with DNP basis set and exchange–correlation functional of B3LYP (Becke exchange plus Lee-Yang-Parr correlation) (Becke, 1992). The following criteria were used to carry out the geometry optimization procedure: the maximum force, energy, displacement tolerances, and maximum iterations were 10^{-5} Ha, 2×10^{-3} Ha•Å^{-1}, 5×10^{-3}Å and 1000 respectively. The self-consistent field (SCF) was calculated with an accuracy of 10^{-6}, and a thermal smearing parameter of 0.005 Ha was applied. The E_{HOMO} and E_{LUMO} values are directly extracted from the output files.

3. Result and discussions

3.1. OCP evaluations

OCP, or open circuit potential, is the free potential between the working and reference electrodes in the absence of any external current flowing through the circuit. It is the quasi-equilibrium potential where the rates of anodic and cathodic reactions are assumed to be equal. The dominant anodic reaction during the acid corrosion of steel is oxidation of iron, whereas the fundamental cathodic reaction is reduction of acidic protons. Therefore, determining the OCP is sacrosanct prior to any electrochemical corrosion measurement. To obtain a steady state OCP, the mild steel (working electrode) was allowed to corrode freely in the acid medium for 30 min. The plots in Fig. 1 reveal that the addidition of EDTP, DITP, and DPTP causes an anodic shift of the steel OCP. Such mechanism indicates the preference of the inhibitors to slow down anodic oxidation (which is the dominant cause of material loss during the corrosion). Suppression of this anodic process invariably shunts the electron transfer between anodic and cathodic sites, which also diminishes the rate of reduction reaction. From Fig. 1, the OCP displacement appears to be concentration dependent, which implies that increased inhibitor concentration favors stronger adsorption and surface coverage of the steel surface. In comparison, the anodic OCP displacement, especially at maximum concentration, is more pronounced in the presence of DPTP and least pronounced with EDTP. This observation strongly suggests that a nitrogen based substituent group promotes stronger interaction between the pyrimidine derivative and the steel surface.

3.2. EIS study

Impedance measurements were conducted for the steel in uninhibited and inhibited 1.0 M HCl solution at OCP to obtain further data regarding the interfacial interaction. Fig. 2(a) shows the Nyquist plot for the mild steel sample in 1.0 M hydrochloric acid without and with various inhibitor concentrations. The Nyquist plots have the shapes of single semicircles, typical of a charge transfer-controlled corrosion mechanism. The inhibitors do not change, but improve this mechanism (Ahmed et al., 2018). The depressed nature of the semicircles is a result of inhomogeneities and roughness of corroding metal surface, which causes a frequency dispersion of the impedance signals (Al-Amiery et al., 2014). Since the size of Nyquist semicircles is a measure of corrosion resistance, DPTP and EDTP obviously provided the highest and least protection, respectively, in agreement with OCP observation. The values of Bode absolute impedance plots in Fig. 2(b) agrees with the Nyquist values.

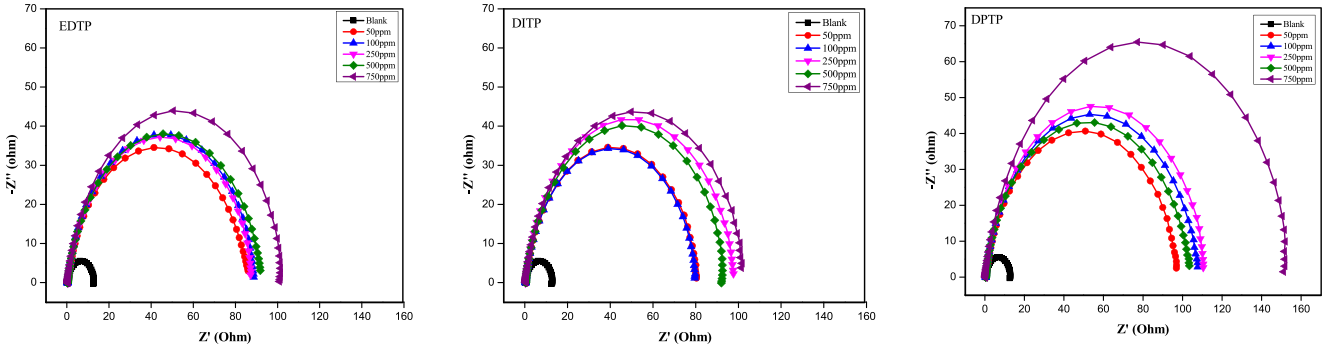

Fig. 2a. Nyquist plot for the corrosion inhibition of mild steel in 1.0 M HCl at 298 K without and with various concentrations of EDTP, DITP and DPTP.

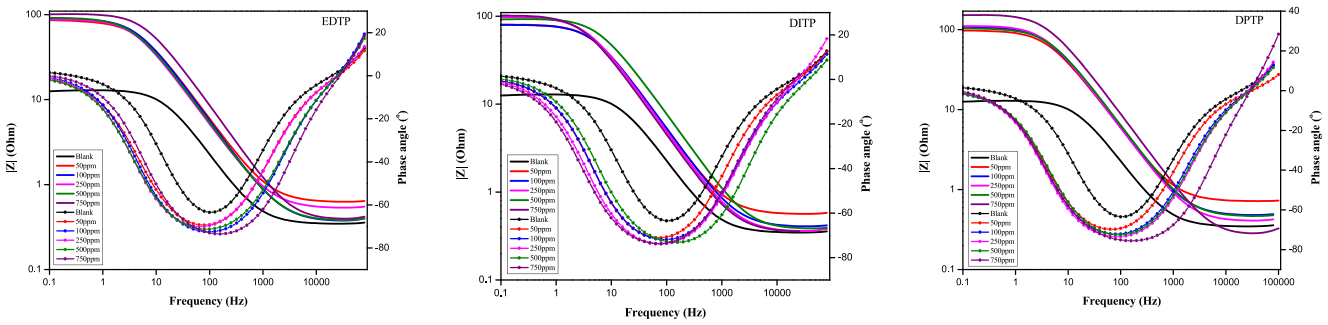

Fig. 2b. Bode plots for the corrosion inhibition of mild steel in 1.0 M HCl at 298 K without and with various concentrations of EDTP, DITP and DPTP.

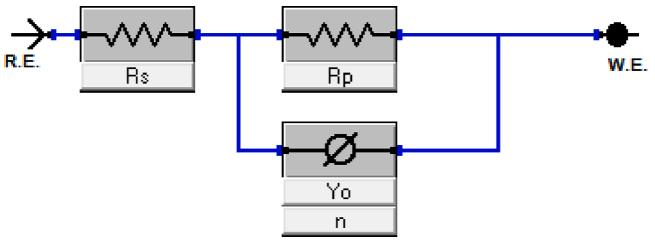

Fig. 2c. An equivalent circuit model for impedance data of the studied system.

The Bode phase plot provides the perfect impedance value and the phase shifts as a function of frequency. The Bode phase diagram for anticorrosion of mild steel in 1.0 M HCl at varying doses of EDTP, DITP and DPTP are also depicted in Fig. 2(b). In Fig. 2(b) (Bode plot) corrosion resistance is established by both the phase angle at high frequencies and the |Z| at low frequencies. Furthermore, in all three inhibitor cases, the value of the |Z| with inhibitor is higher than those of the uninhibited mild steel specimen, representing an excellent efficiency of the inhibitors by the blockade to corrosion medium dispersion. Additionally, as depicted in Fig. 2(b) (Bode plot), the phase angle at higher frequency with inhibitor is about 65o larger than that of uninhibited mild steel, signifying that the mild steel coated with the inhibitor layer having strong interfacial contact. Also in Fig. 2(b), the associated Bode phase angle plots show single peaks for steel in both uninhibited and inhibited HCl solution. The single phase-angle peak is consistent with an activation-controlled corrosion, and the peak heights increase with inhibitor concentration such that maximum peak height occurs with 750 ppm of each inhibitor, with DPTP delivering the highest efficiency.

The shapes of Nyquist and phase angle plots compel us to adopt the simple Randle's circuit (Fig. 2(c)) as an electrical circuit model to describe the impedance (corrosion) phenomenon. The use of a constant phase element (CPE), in lieu of a pure capacitor (C_{dl}), is because of the surface roughness and heterogeneity of the corroding steel. The circuit consists of a solution resistance (R_s), CPE constant (Y_o), CPE roughness parameter (n), and polarization/charge transfer resistance (R_p) (Obot et al., 2020; Ech-Chihbi et al., 2020). The Eq. (1) defines the impedance of a CPE; whereby ω and j indicate the angular frequency (2πf) and an imaginary number, respectively. However, double layer capacitance (C_{dl}) usually provides better description of the steel-solution interfacial phenomenon, and it can be deduced from the CPE based on Eq. (2) (Idris et al., 2013). The values of these electrical elements obtained upon fitting the impedance results with the circuit model are in Table 1.

$$Z_{CPE} = \frac{1}{Y_0 \times (j \times \omega)^n} \quad (1)$$

$$C_{dl} = \frac{(Y_0 \times R_p)^{1/n}}{R_P} \quad (2)$$

$$\text{Inhibition Efficiency (IE \%)} = \frac{R_{p\,(Inh)} - R_{p\,(B)}}{R_{p\,(Inh)}} \times 100 \quad (3)$$

$$\text{Fractional surface coverage } (\theta) = \frac{R_{p\,(Inh)} - R_{p\,(B)}}{R_{p\,(Inh)}} \quad (4)$$

Table 2 shows that higher inhibitor concentrations cause continuous increase in the R_p, and decrease in C_{dl}. The relationship between R_p values in the uninhibited and inhibited acid solutions enables the calculation of the inhibition efficiency (IE %) and extent of surface coverage (θ) by the inhibitor, based on Eq. (3), 4). Accordingly, the IE % for DPTP (91.7 %) was higher than that of the DITP (87.7 %) and EDTP (87.6 %) at 750 ppm. These results confirm that the synthesized pyrimidine derivatives (EDTP, DITP, and DPTP) possess remarkable

Table 2
Impedance parameters of mild steel in 1.0 M HCl containing different concentrations of EDTP, DITP and DPTP at 298K.

Medium	Concentration (ppm)	R_s (Ω/cm^2)	R_p (Ω/cm^2)	Y_o ($S*s^n$)	n	C_{dl} (μF)	θ	IE (%)
1M HCl	0	0.3477	12.62	0.0013	0.9083	849.04		-
EDTP	50	0.6235	84.95	0.0006	0.8767	396.42	0.85	85.14
	100	0.3745	89.27	0.0006	0.8922	394.85	0.86	85.86
	250	0.5342	88.76	0.0007	0.8783	466.26	0.86	85.78
	500	0.3782	92.25	0.0007	0.8775	445.23	0.86	86.32
	750	0.3911	102.00	0.0003	0.9028	244.94	0.88	87.63
DITP	50	0.5642	80.72	0.0006	0.8975	423.19	0.84	84.37
	100	0.4056	80.39	0.0006	0.8930	418.49	0.84	84.30
	250	0.3603	98.19	0.0006	0.8985	459.00	0.87	87.15
	500	0.3805	93.41	0.0004	0.8986	274.50	0.86	86.49
	750	0.3569	102.80	0.0007	0.8955	514.33	0.88	87.72
DPTP	50	0.7142	97.36	0.0006	0.8839	397.71	0.87	87.04
	100	0.4771	107.80	0.0005	0.8895	385.06	0.88	88.29
	250	0.4064	111.70	0.0005	0.8967	383.25	0.89	88.70
	500	0.4627	103.10	0.0005	0.8915	354.87	0.88	87.76
	750	0.2781	152.90	0.0003	0.9041	249.84	0.92	91.75

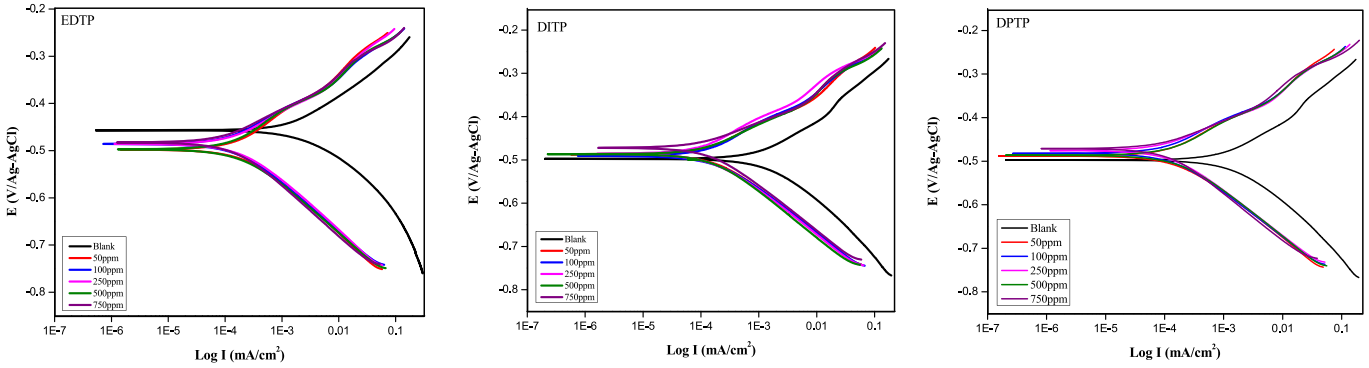

Fig. 3. Polarization curves for the corrosion inhibition of mild steel in 1.0 M HCl with and without different concentrations of EDTP, DITP and DPTP at 298 K.

Table 3
Potentiodynamic polarization parameters for mild steel in 1.0 M HCl containing different concentrations of EDTP, DITP and DPTP at 298K

Compound	Conc. (ppm)		PDP					LPR	
		i_{corr} (μA/cm²)	$-E_{corr}$ (mV/Ag-AgCl)	β_a (V/decade)	$-\beta_c$ (V/decade)	CR (mpy)	IE (%)	R_p (Ω/cm²)	IE (%)
1 M HCl	0	1110	498	0.0952	0.0943	194.20	-	11.72	-
EDTP	50	226	498	0.1331	0.1049	19.44	79.64	85.02	86.22
	100	148	486	0.0952	0.0980	12.67	86.67	92.87	87.38
	250	172	486	0.0972	0.0987	14.76	84.50	87.83	86.66
	500	185	497	0.1241	0.0992	15.92	83.33	92.99	87.40
	750	125	483	0.0815	0.1015	10.76	88.74	106.3	88.97
DITP	50	142	487	0.0862	0.0924	26.99	87.21	84.32	86.10
	100	150	491	0.0954	0.0901	26.92	86.49	84.55	86.14
	250	129	486	0.1019	0.0936	22.45	88.38	97.37	87.96
	500	131	487	0.0770	0.0989	24.19	88.20	94.09	87.54
	750	125	472	0.0672	0.0972	23.38	88.74	101.4	88.44
DPTP	50	143	488	0.1028	0.0972	22.16	87.10	102.7	88.59
	100	125	482	0.0913	0.0983	20.34	88.70	111.9	89.53
	250	121	476	0.0843	0.0992	19.2	89.10	118.6	90.12
	500	133	487	0.0823	0.0951	21.9	88.00	103.9	88.72
	750	110	471	0.0688	0.1078	15.99	90.10	142.4	91.77

inhibitory performance for mild steel in acid medium. At OCP, the corrosion rate of the mild steel in the acid solution depends on the charge composition/concentration within the steel-solution interfacial double layer, and the rate of charge transfer across this double layer. In the uninhibited acid solution, the double layer majorly contains H_2O, H^+ and Cl^- ions, all of which increase the rate of corrosion by promoting the release of Fe^{2+} and reduction of H^+. In the presence of the pyrimidine derivatives, the inhibitor molecules have the capability to adsorb onto the steel surface using its N and O heteroatoms (and/or pi-electrons from cyclic/aromatic rings) as interaction centers. Once adsorbed, they displace H_2O molecules and other ionic species like H^+ and Cl^- ions. The organic films they subsequently establish hydrophobic status that shields the steel surface from further corrosion attack. Thus, the inhibitors decrease the concentration of aqueous species/charges occupying the interfacial double layer and the rate of charge transport across the interface. This is evident in the continuously lower C_{dl} and higher R_p values in the presence of inhibitors. However, N-based organic corrosion inhibitors exhibit stronger filming capability (Obot et al., 2019b). Therefore, the extra N atom and pi-electrons in the NHC_6H_5 substituent explains why DPTP displays greater efficiency than DITP and EDTP. Although the presence of O-based substituent in EDTP should favor greater interaction and adsorption compared with DITP, the bulky C_2H_5 group (compared with a simple CH_3) could induce some steric hindrances against DITP adsorption.

3.3. Study of Tafel polarization

During corrosion of the steel in 1.0 M HCl without and with different concentrations of EDTP, DITP and DPTP, the linear polarization resistance (LPR) and potentiodynamic polarization (PDP) measurements yield the following plots in Fig. 3 and data in Table 3. The Polarization parameters from both techniques, such as corrosion current density (i_{corr}), corrosion potential (E_{corr}), corrosion rate (CR), cathodic Tafel slope (β_c), and anodic Tafel slope (β_a) were extrapolated ± 10 mV around the OCP. The derivation of polarization resistance (R_p) followed Eq. (5), and the IE % was determined based on Eq. (6) & (7), whereby $i_{corr(B)}$ and $i_{corr(inh)}$ indicate the current density in the uninhibited and inhibited solution, respectively, (Ammal,Prajila,and Joseph, 2018). Although the LPR is a non-destructive technique that measures instantaneous corrosion rate by gently polarizing the steel away from OCP, it is incapable of elucidating the actual corrosion/corrosion inhibition mechanism. This is achievable with the PDP, which traditionally applies greater potential displacement from OCP.

$$\text{Polarization resistance}\left(R_p\right) = \frac{\beta_c \times \beta_a}{2.3\left(\beta_c + \beta_a\right) \times i_{corr}} \quad (5)$$

$$\text{Inhibition Efficiency}\,(IE\%) = \frac{i_{corr\,(B)} - i_{corr\,(Inh)}}{i_{corr\,(B)}} \times 100 \quad (6)$$

$$\text{Inhibition Efficiency}\,(IE\%) = \frac{R_{p\,(Inh)} - R_{p\,(B)}}{R_{p\,(Inh)}} \times 100 \quad (7)$$

When inhibitors are not present, the rate of steel degradation due to corrosion is higher than that of the inhibited steel specimen. This occurs by the concentration-dependent lowering of i_{corr} and CR in the presence of inhibitors. As a steady state technique measured at OCP, the R_p values derived from LPR measurement shows strong closeness to the R_p values

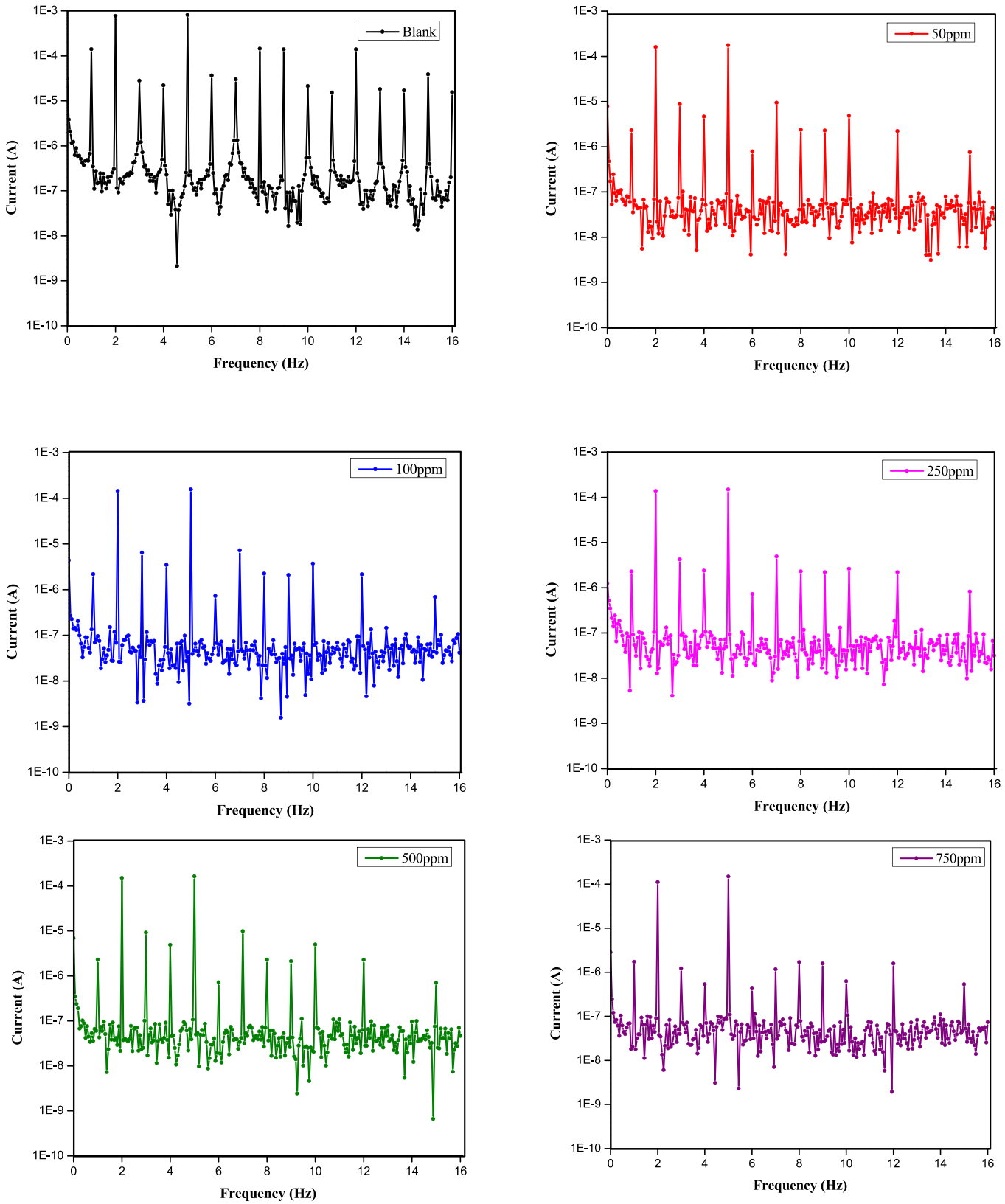

Fig. 4. Intermodulation spectrum for mild steel in 1.0 M HCl solutions without and with various concentrations (50–750 ppm) of DPTP at 298 K.

measured by EIS. From Fig. 3, all the tested inhibitors exhibit mixed-type characteristics such that they have minimal effect on the E_{corr} but shift both anodic and cathodic current density to lower values. The cathodic currents diminish because the protonated inhibitors can co-adsorb on cathodic sites in competition with H^+ ions. Their adsorption increases the inertness of cathodic sites and lowers the extent of electrons demand from anodic sites. Simultaneously, the protonated inhibitors can also lower the activities at anodic sites by supplying their pi-

Table 4
Electrochemical kinetic parameters obtained by EFM technique for mild steel in 1.0 M HCl solutions at different concentrations of the EDTP, DITP and DPTP at 298K

Compound	Conc. (ppm)	β 1 (V/decade)	-β 2 (V/decade)	C.R (mpy)	CF-2	CF-3	IE%
1 M HCl	0	0.0351	0.0404	170.6	1.57	3.93	-
EDTP	50	0.0864	0.1487	28.51	1.96	2.99	83.29
	100	0.0840	0.1127	22.84	1.91	3.06	86.61
	250	0.0846	0.1175	24.73	1.92	3.09	85.50
	500	0.0830	0.1336	24.7	1.93	2.85	85.52
	750	0.0914	0.1190	22.01	1.93	3.02	87.10
DITP	50	0.0846	0.1061	24.5	1.92	2.98	85.64
	100	0.0836	0.1142	25.38	1.93	3.14	85.12
	250	0.0795	0.1089	20.45	1.95	2.89	88.01
	500	0.0916	0.1145	23.27	1.90	2.93	86.36
	750	0.0819	0.0897	19.15	1.92	2.98	88.77
DPTP	50	0.0879	0.1239	23.27	1.92	2.97	86.36
	100	0.0866	0.1142	19.89	1.89	3.06	88.34
	250	0.0854	0.1025	17.95	1.83	2.91	89.48
	500	0.0851	0.1245	21.28	1.92	3.17	87.53
	750	0.0995	0.1054	17.77	2.06	3.42	89.58

Table 5
Comparison of the inhibitory efficiency of previously reported compounds with EDTP, DITP and DPTP

Inhibitor	Corrosive Medium	Concentration of Inhibitor	IE (%)		Reference
			EIS	PDP	
5-Acetyl-4-[4-(dimethylamino)phenyl]-6-methyl-3,4-dihydropyrimidin-2(1*H*)-one	1.0 M HCl	0.0025 M	85.0	88.0	Rasheeda et al., 2022a
2-(((3,5-Dimethyl-1*H*-pyrazol-1-yl)methyl)amino)-6-methylpyrimidin-4-ol	1.0 M HCl	0.001 M	85.4	86.8	Elmsellem et al., 2014
Ethyl (5-methyl[1,2,4]triazolo[1,5-a]pyrimidin-7-yl)acetate	1.0 M HCl	0.001 M	84.0	87.0	Lahmidi et al., 2017
6-Amino-3,4-dihydropryimidin-2(1*H*)-thione	1.0 M HCl	0.001 M	73.0	71.0	Abdelazim et al., 2021
2-(((2,3-Dihydro1*H*-pyrazol-1yl)methyl)amino)pyrimidine-4,6-diol	1.0 M HCl	0.001 M	77.0	81.0	Arrousse et al., 2020
7-Methoxypyrido[2,3-*d*]pyrimidin-4-amine	2.0 M HCl	0.005 M	72.9	-	Yadav et al., 2015
4,6-Dimethylpyrimidine-2-amine	2.0 M HCl	0.005 M	71.2	-	Elewady, 2008
EDTP (Present study)	1.0 M HCl	0.0025 M (750 ppm)	87.63	88.74	
DITP (Present study)	1.0 M HCl	0.0025 M (750 ppm)	87.72	88.74	
DPTP (Present study)	1.0 M HCl	0.0025 M (750 ppm)	91.75	90.10	

electrons and lone pair electrons (around N and O) to interact with the empty d-orbitals in the Fe/Fe^{2+} species. The resultant coordinate covalent bonding leads to the formation of an inhibitor film that shunts the release of electrons from the anode. In addition, the abundance of Fe^{2+} cations at the anodic sites can attract some Cl^- ions to form a primary adsorbed layer that, in turn, attracts the protonated inhibitors to the anode. On this basis, it suggests that the additional N group in DPTP favours more stable protonation and stronger interaction with the steel substrate. Previous works have also confirmed that the substitution of an OH group with $N(CH_3)_2$ group significantly improved the corrosion resistance of pyrimidine derivatives in an acidic CO_2-saturated solution (Onyeachu et al., 2019; Onyeachu, Quraishi, and Obot 2023b).

3.4. EFM studies

Electrochemical Frequency Modulation (EFM) is a non-destructive corrosion measurement technique that combines alternating current and direct current measurements to determine the corrosion current density without prior knowledge of the Tafel constants (Kuş and Mansfeld, 2006). Fig. 4 provides the representative intermodulation spectra obtained from the EFM measurements of the steel corrosion in 1.0 M HCl without and with different concentrations of DPTP. Table 4 displays the kinetic parameters extrapolated from the measurements with all the tested inhibitors. As in Fig. 4, the two peaks with amplitude in the range of 100 μA are the responses to the excitation frequencies of 2 Hz and 5 Hz. The peaks observed between 1 μA and 10 μA are the harmonics, differences and sums of two excitation frequencies. The accuracy of the presented data in Table 4 lies in the agreement between the CF 2 and CF 3 values with the theoretical values of 2 and 3 (Rehim et al., 2008). In addition, the inhibition efficacy of EDTP, DITP, and DPTP increases with

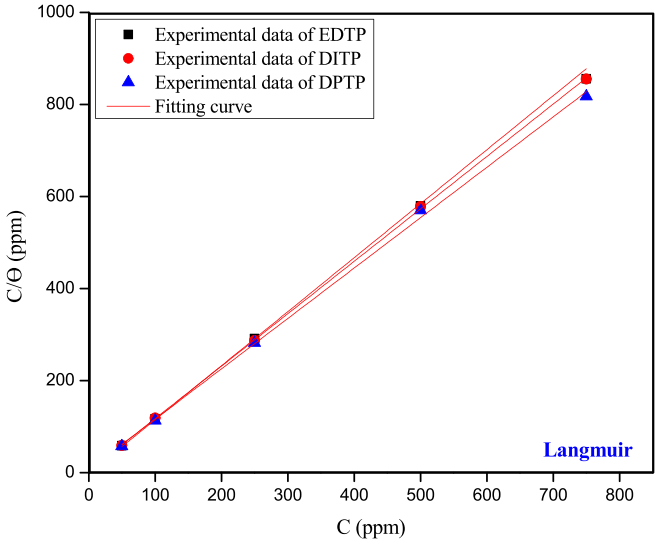

Fig. 5. Langmuir isotherm plot for the adsorption of EDTP, DITP and DPTP on the surface of mild steel determined by electrochemical impedance spectroscopy.

the inhibitor concentration and displays the highest inhibition efficacy at an optimal concentration of 750 ppm. Hence, the data obtained from the EFM technique matches well with the result obtained from other electrochemical measurements. The result also confirms the best performance of DPTP amongst the pyrimidines. The results observed for the anticorrosion properties of EDTP, DITP, and DPTP by various

Table 6
Calculated values of K_{ads} and ΔG^{o}_{ads} from various isotherms for mild steel in 1.0 M HCl solution containing EDTP, DITP and DPTP at 298K

Isotherms	Inhibitor	R^2	K_{ads} (M^{-1})	ΔG^{o}_{ads} ($kJmol^{-1}$)
Langmuir	EDTP	0.9998	79905.4	-37.93
	DITP	0.9999	71054.7	-37.63
	DPTP	0.9988	52374.2	-36.88
Freundlich	EDTP	0.4120	-2732917.6	-
	DITP	0.7567	-1177992.1	-
	DPTP	0.3408	-1849031.6	-
Frumkin	EDTP	0.3459	3899.4	-30.44
	DITP	0.8013	-4977.5	-
	DPTP	0.4848	-8496.9	-
EL-Awady	EDTP	0.4123	329235.6	-41.43
	DITP	0.7515	501057.9	-42.47
	DPTP	0.3212	570041.9	-42.79
Flory-Huggins	EDTP	0.4206	-23262.7	-
	DITP	0.7431	53273.1	-36.92
	DPTP	0.3016	201879.9	-40.22
Temkin	EDTP	0.4120	337926.6	-41.50
	DITP	0.7559	344237.4	-41.54
	DPTP	0.3384	423346.2	-42.06

electrochemical techniques were compared with existing literature (Table 5). The data shows that EDTP, DITP, and DPTP have better corrosion inhibitive effects than inhibitors that were found in the literature.

3.5. Isotherm for adsorption

The inhibition mechanism of metals and inhibitors is typically described by adsorption isotherms (Akinbulumo,Odejobi,and Odekanle, 2020). The θ values gained from electrochemical analyses were utilized to plot different adsorption isotherms. The data fits the Langmuir adsorption model (Fig. 5) well out of the examined isotherms (Flory-Huggins, EL-Awady, Freundlich, Langmuir, Temkin, and Frumkin) as shown in the supplemental data, Fig. S1. Equation (8) relates the values of θ and the concentration (C) of EDTP, DITP, or DPTP to the equilibrium adsorption constant K_{ads} in the Langmuir model (Lai et al., 2017).

$$\frac{C}{\theta} = \frac{1}{K_{ads}} + C \tag{8}$$

The Langmuir adsorption model revealed high degree of linearity with a correlation coefficient (R^2) = 0.999 that is nearly equal to 1 (Table 6). It proves that all the synthesized compounds follow the Langmuir adsorption model (Chakravarthy and Mohana, 2014). Furthermore, values of K_{ads} and ΔG_{ads} can be determined by using the following equations:

$$K_{ads}\left(M^{-1}\right) = \frac{\text{Molecular weight of inhibitor} \times 1000}{\text{Intercept Value (in mg/l)}} \tag{9}$$

$$\Delta G^{0}_{ads} = -2.303\,RT \times \log\left(55.5 \times K_{ads}\right) \tag{10}$$

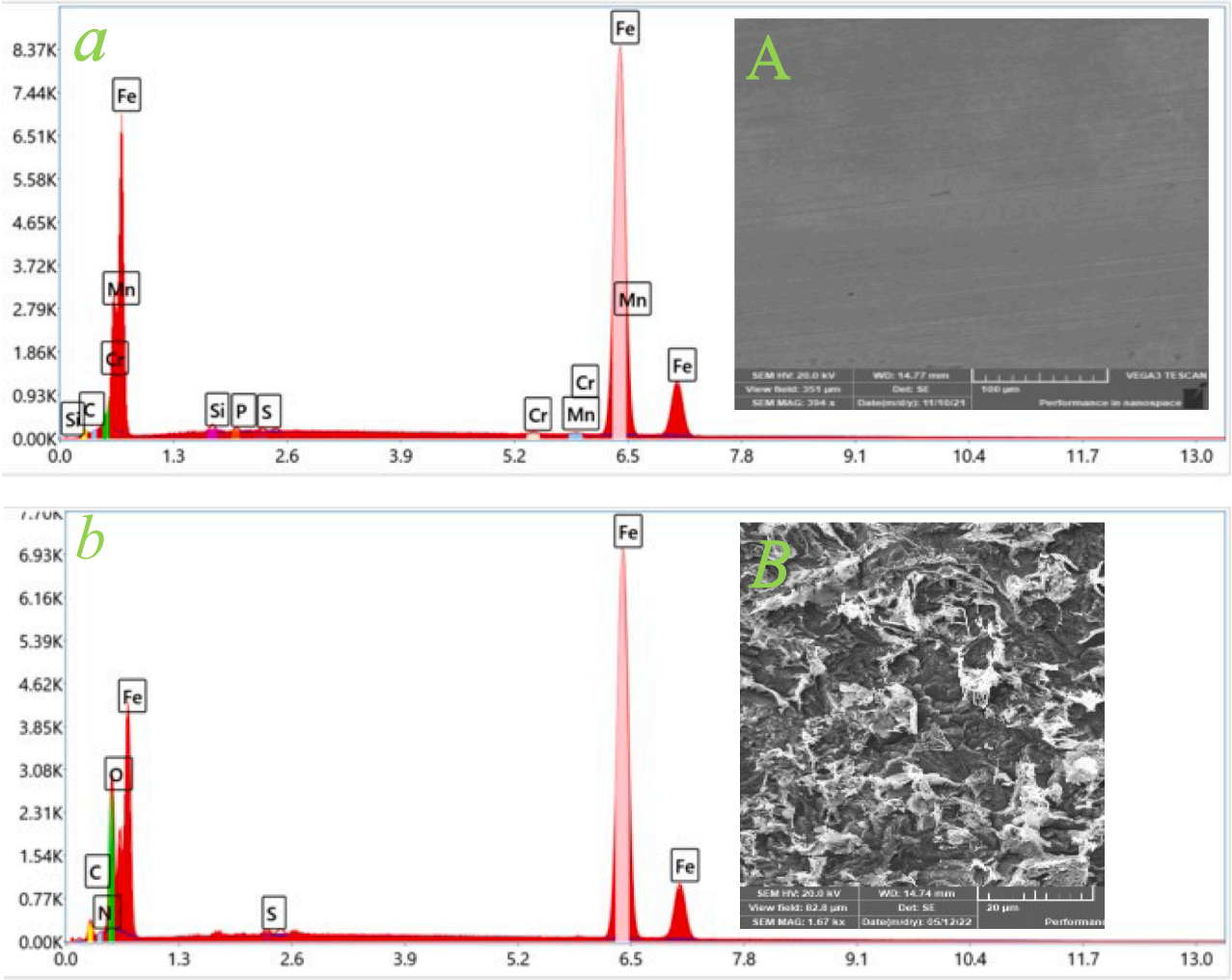

Fig. 6. SEM (A-E) and EDX (a-e) images of mild steel surface before (A-a; polishing) and after immersion for 12 h in 1.0 M HCl solution at 298 K in the absence and existence of 750 ppm of inhibitors: (B-b; blank), (C-c; EDTP), (D-d; DITP), (E-e; DPTP).

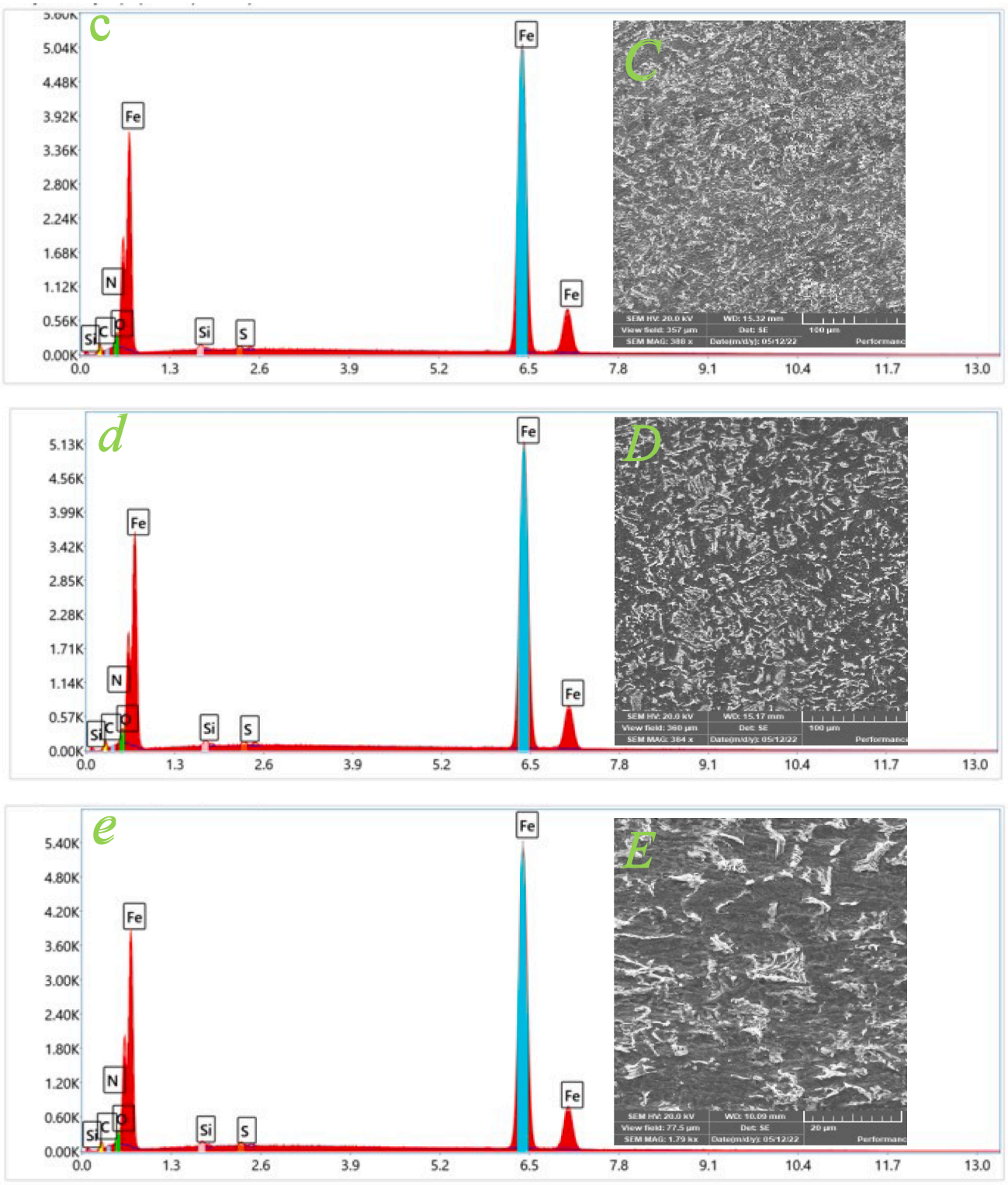

Fig. 6. (*continued*).

where T and R denote the absolute temperature, and gas constant (8.314 $JK^{-1}mol^{-1}$), respectively, and 55.5 indicates the water concentration in molarity. A ΔG^{o}_{ads} value equal to or greater than −20 $kJmol^{-1}$ indicates physisorption relating to electro-static interaction of the charged metal with the charged inhibitor. On the other hand, chemisorption occurs when the ΔG^{o}_{ads} value is equal to or below −40 $kJmol^{-1}$ due to the charge transfer between inhibiting molecule and the metal surface (Praveen et al., 2021). As described in Table 6, the values of ΔG^{o}_{ads} for DPTP, EDTP, and DITP are −36.88 $kJmol^{-1}$, 37.93 $kJmol^{-1}$, and −37.63 $kJmol^{-1}$, respectively, which designate the adsorption of all three pyrimidine derivatives on the metallic surface following the blended mechanism (chemisorption and physisorption). The inclination of the inhibitors to adsorb according to the Langmuir isotherm shows that they majorly form simple monolayer of their films during corrosion inhibition, and that no inhibitor-inhibitor interaction exists. This could also explain the single time constant v c why consistent with the Randles

Table 7
Results obtained from EDX analysis for the inhibitory effect of EDTP, DITP and DPTP on mild steel.

Elements	Weight %				
	Mild steel	Mild steel in 1.0 M HCl	Mild steel in EDTP	Mild steel in DITP	Mild steel in DPTP
C	0.0	5.4	3.75	3.80	3.99
N	0.0	0.4	0.00	0.00	0.44
O	0.0	11.8	1.55	1.63	1.56
S	0.3	0.4	0.31	0.39	0.41
Fe	98.2	82.0	93.85	93.60	93.01
Si	0.7	0.0	0.54	0.59	0.58
P	0.3	0.0	0.00	0.00	0.00
Cr	0.2	0.0	0.00	0.00	0.00
Mn	0.3	0.0	0.00	0.0	0.00

equivalent model where only a single time constant was observed in the EIS results.

3.6. Surface analysis

Scanning electron microscopy (SEM) is an important technique for characterizing the effect of an inhibitor on the corrosion-induced destruction of the steel surface morphology. Fig. 6 (A-E) illustrates the SEM images of the mild steel surface before and after the immersion for 12 h in 1.0 M hydrochloric acid with and without the presence of 750 ppm of inhibitors EDTP, DITP, and DPTP, respectively. Fig. 6 (A) depicts the smooth and non-corroded surface of the pure steel. As illustrated in Fig. 6 (B), without the inhibitor, the mild steel surface exhibits a significantly higher level of microstructural damage, indicating that mild steel shows enhanced metal dissolution in an acidic media. Furthermore, when treated with 750 ppm of EDTP (Fig. 6 (C)), DITP (Fig. 6 (D)), and DPTP (Fig. 6 (E)) in 1.0 M HCl, a mild steel surface exhibits smoother morphologies than the uninhibited surface. On the other hand, the mild steel surface displays much less corrosion by forming a shielding film and is comparatively more homogenous in the occurrence of DPTP (Tiongson et al., 2020). EDX (Energy dispersive X-ray spectroscopy) analysis was also conducted to discover the elemental composition on the surface of the tested samples. The observed spectral results are depicted in Fig. 6 (a-e). The proportion of numerous atoms adsorbed on the metallic surface is illustrated in Table 7. As displayed in Fig. 6 (a), the EDX spectra expose a low peak for oxygen and a high peak for iron, which indicates a corrosion-free surface. The interpretation of spectrum (b) (Fig. 6 (b)) discloses that iron oxide is achieved via the corrosion method, which is confirmed by the presence of the highest oxygen peak in the mild steel EDX spectra. However, oxygen peak is extremely decreased by adding inhibitors EDTP, DITP, and DPTP, respectively, as illustrated in Fig. 6 (c), (d), and (e). These observations reveal the inhibitory properties of all three synthesized inhibitors by creating the preventative film over the metal surface and hence reducing the corrosion phenomena (Mahendra Yadav *et al.* 2015).

3.7. DFT descriptors

DFT analysis was carried out to correlate the inhibitor's corrosion inhibition efficiency and structure. The HOMO (Highest Occupied Molecular Orbital) and LUMO (Lowest Unoccupied Molecular Orbital) are the two major descriptors in the theoretical segment. A higher E_{HOMO} value shows the strength of the inhibitor to form coordinate bond with the metal. In contrast, a lower E_{LUMO} value indicates the strength of the inhibitor in acquiring feedback bonds from metal (Guo et al., 2017). The optimized structure, HOMO, LUMO, and molecular electro-static potential (ESP) for EDTP, DITP and DPTP are displayed in Fig. 7. The E_{HOMO} value for EDTP (-5.1548 eV), DITP (-5.1568 eV) and DPTP (-5.2669 eV) indicating that all the inhibitors have the similar donating ability, but slightly higher for EDTP molecule. Moreover, as displayed in Fig. 7, E_{LUMO} of all the inhibitors has almost equal values but is relatively low for DITP (-1.1534 eV) molecule.

Typically, when the energy gap (ΔE) is smaller as shown in (Table 8) the inhibitor shows performance in terms of inhibition (Junaedi et al., 2013). This suggests that the energy gaps, for EDTP, DITP and DPTP produce outcomes, which aligns with what has been observed. Furthermore (Table 8) also presents another factor called ΔN (fraction of transferred electrons) which is used to assess activity. As per the literature inhibition effectiveness improves when ΔN is, below 3.6 indicating an ability to release electrons onto the metal surface (Ferigita et al., 2022). Hence all three inhibitors exhibit results that support the data. In the ESP diagrams, the blue region indicates the nucleophilicity, and the yellow region denotes the electrophilicity of a molecule (Sliem et al., 2020). As depicted in Fig. 7, different atoms of three inhibitors contribute to the nucleophilicity and electrophilicity of those molecules, enabling the coordinate and feedback bonds with metal.

3.8. Fukui index analysis

The Fukui indices provide information regarding the reactive sites accountable for donor–acceptor adsorption between metal and inhibitors. The nucleophilic (f_k^+) and electrophilic (f_k^-) attacks of EDTP, DITP, and DPTP as per Mulliken and Hirshfeld population analysis at BLYP/DNP level are tabularized in the supplementary file, Table S1. The atom with utmost f_k^+ value discloses the preferred site to experience a nucleophilic attack. In contrast, the atom with the highest f_k^- value displays the desired site for the electrophilic attack (Oguike et al., 2013).

Both analyses of indices are specified in Table S1. In EDTP, the atom designated N(18) is the favored for an electrophilic attack, but in DITP and DPTP, the atom designated N(16) is the ideal site for an electrophilic attack. Similarly, for nucleophilic attack, the atoms designated C(12), O (15), and C(14) present in EDTP, DITP, and DPTP are the most reactive sites (Fig. S2).

3.9. Monte Carlo modelling

In this study a Monte Carlo simulation was performed to investigate how EDTP, DITP and DPTP molecules arrange themselves on the surfaces of steel. Fig. 8 displays the configuration of these molecules, in the Fe (1 1 0) / 100 H_2O systems.

As can be visible from Fig. 8, the simulation of all three inhibitors adsorbs through parallel orientation on Fe (1 1 0) surface through the pyrimidine ring and the benzene ring containing dimethyl amino group. It is evident from Table 9 that **DPTP** shows a high negative number of adsorption energy (which may be due to the presence of NH-C_6H_5 group) during the simulation process. Maximum adsorption energy values imply that **DPTP** inhibitors will provide slightly higher inhibition efficiency than EDTP and DITP (Saadouni et al., 2018). This further concludes that the theoretical investigations align with the experimental results.

3.10. Adsorption mechanism

The combined results of both theoretical and experimental studies suggest that the compounds EDTP, DITP and DPTP can act as inhibitors against corrosion on iron surfaces in 1.0 M HCl by adsorbing onto them. It is clear that the adsorption of these three pyrimidine derivatives on the metal surface occurs directly relying on the pi-electrons present in the pyrimidine structure and the interaction between the pairs of heteroatoms and vacant d-orbitals of the metal atoms. Additionally, the presence of dimethyl amino group in these compounds improves electron density, on their heterocyclic ring.

In acidic conditions, these inhibitors can exist as protonated species. These protonated species have the ability to adsorb onto the cathodic sites of the mild steel surface and reduce hydrogen evolution. Additionally, they can adsorb onto anodic sites through electron-rich

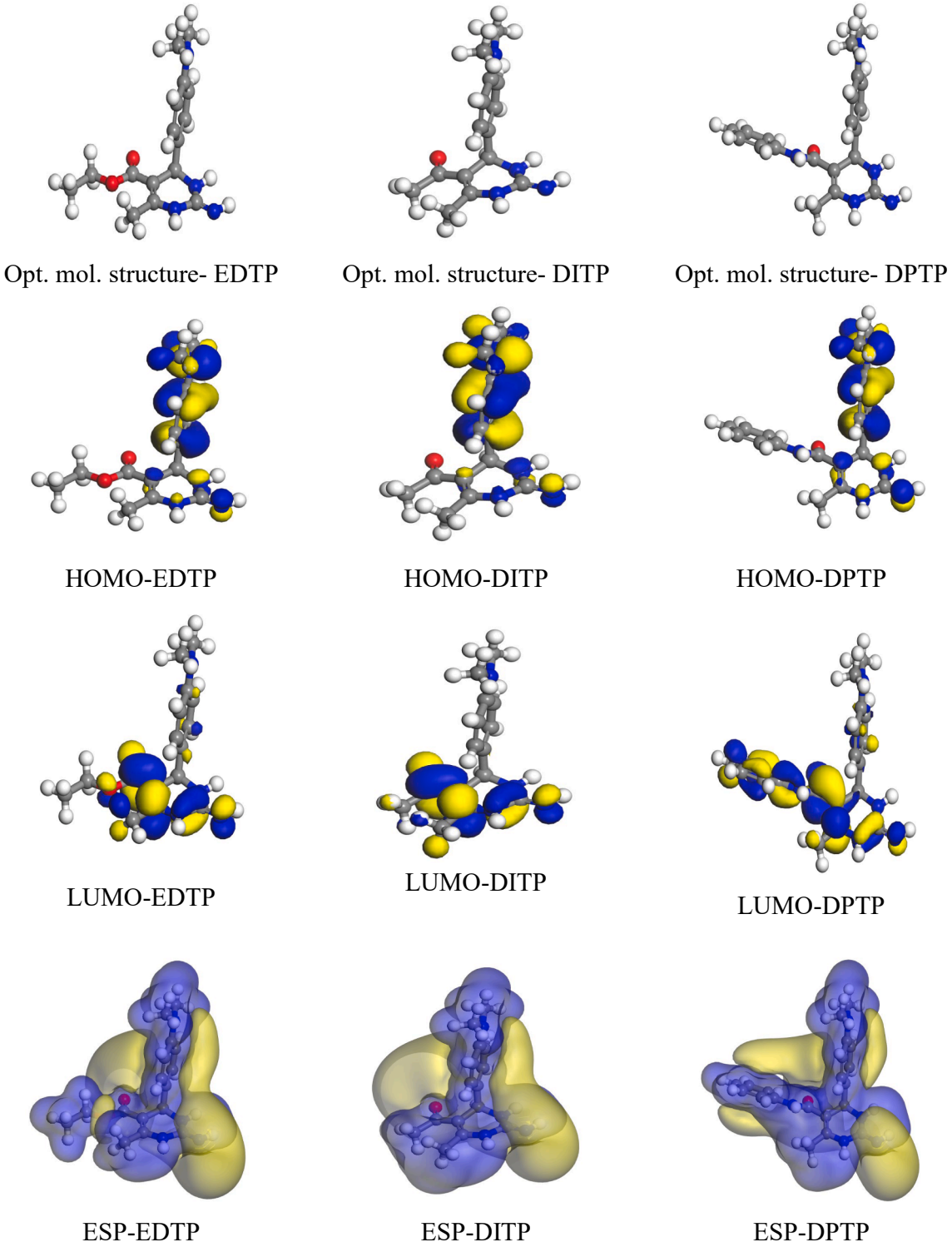

Fig. 7. Optimized structure, HOMO, LUMO, and molecular electrostatic potential (ESP) of EDTP, DITP and DPTP molecules obtained from quantum chemical results using the GGA/BLYP/DNP level of theory.

Table 8
Calculated quantum chemical descriptors for EDTP, DITP and DPTP by DFT computation study in gas phase.

Inhibitor	HOMO (eV)	LUMO (eV)	I(eV)	A(eV)	ΔE (eV)	χ(eV)	η(eV)	S(eV^{-1})	ω(eV)	ΔN
EDTP	-5.1548	-0.8396	5.1548	0.8396	4.3152	2.9972	2.1576	0.4635	1.0409	0.4224
DITP	-5.1568	-1.1534	5.1568	1.1534	4.0034	3.1551	2.0017	0.4996	1.24324	0.4159
DPTP	-5.2669	-0.8154	5.2669	0.8154	4.4515	3.0411	2.226	0.4493	1.0388	0.3996

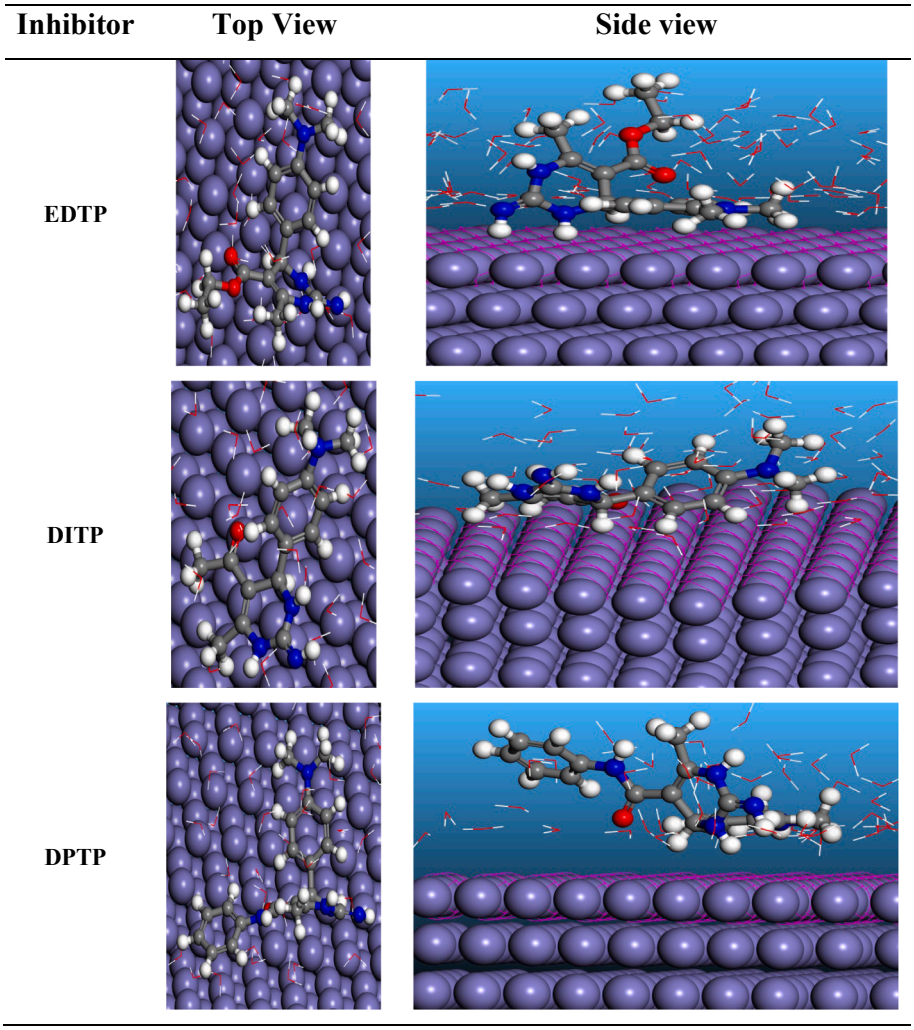

Fig. 8. Top and side views of the most stable configurations for EDTP, DITP and DPTP on Fe (1 1 0)/100 H_2O system.

Table 9
Outputs and descriptors calculated by the Monte Carlo simulation for the most stable adsorption configurations of EDTP, DITP and DPTP molecules on Fe (110)/100 H_2O system (all units in kcal/mol).

Inhibitor	Adsorption energy	Rigid adsorption energy	Deformation energy	Inhibitor: dE_{ad}/dN_i	Water: dE_{ad}/dN_i
EDTP	-1475.116	-1543.674	68.559	-151.228	-14.236
DITP	-1469.189	-1546.981	77.791	-142.657	-10.058
DPTP	-1503.289	-1574.726	71.437	-172.948	-12.594

nitrogen atoms, the dimethyl amino group, aromatic and heterocyclic rings, thereby reducing the anodic dissolution of the metal. The efficiency of these molecules as corrosion inhibitors fundamentally relies on the active centers and the size of the molecule. The relatively superior performance of DPTP as a corrosion inhibitor compared to EDTP and DITP may be attributed to its bulkiness and/or the presence of the –NH-C_6H_5 functionality in DPTP.

The complete results of theoretical and experimental investigations revealed that all three synthesized pyrimidine derivatives prevent the corrosion of the Fe surface in 1.0 M HCl by adsorption mechanism. Based on the results of DFT studies and Fukui indices, the possible mechanism for the adsorption of EDTP, DITP and DPTP on mild steel is proposed (Fig. 9).

4. Conclusion

The findings of this study indicate that the synthesized pyrimidine derivatives, EDTP, DITP and DPTP show promise as anticorrosive agents, for mild steel in a 1.0 M HCl solution. From the obtained results we can draw conclusions. Firstly, the efficiency of these inhibitors in inhibiting corrosion increased with concentrations. Among them DPTP exhibited the efficacy (91.7 %) followed by DITP (87.7 %) and EDTP (87.6 %) at a 750 ppm concentration. Moreover, the presence of these inhibitors reduced the corrosion density from 1110 to 110 μA/cm^2 at 750 ppm indicating their role as inhibitors with mixed properties. The adsorption behavior of these inhibitors complied with the Langmuir isotherm model suggesting both physical and chemical adsorption mechanisms were involved in their action. Confirmation of inhibitor adsorption on the surface was provided by SEM and EDX evaluation, which revealed the formation of a barrier. Additionally, both DFT and MC simulation studies supported our findings by demonstrating the effectiveness of these pyrimidine derivatives as agents.

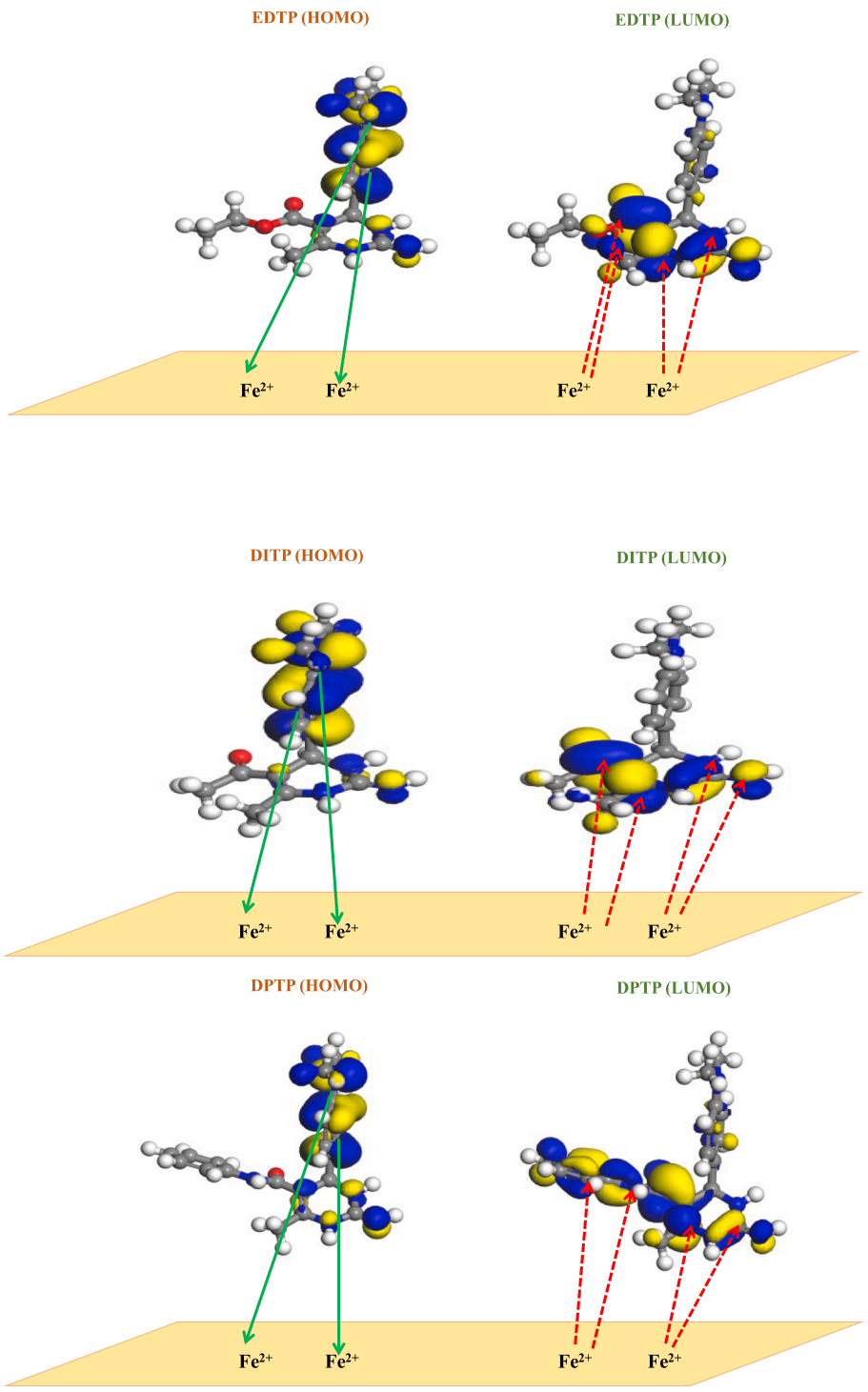

Fig. 9. Proposed schematic representation for the adsorption of EDTP, DITP and DPTP on the metal surface.

CRediT authorship contribution statement

Aeshah H. Alamri: Data curation, Formal analysis, Software, Validation, Writing – original draft. **Kedila Rasheeda:** Formal analysis, Methodology, Validation. **Salwa J. Kamal:** . **Marwah Aljohani:** Data curation, Methodology, Visualization. **Talal A. Aljohani:** Methodology, Validation, Writing – review & editing. **Irshad Baig:** Formal analysis, Software, Visualization. **Vijaya D.P. Alva:** Resources, Validation, Writing – review & editing. **N. Phadke Swathi:** Formal analysis, Methodology, Visualization. **Ikenna B. Onyeachu:** Resources, Writing – review & editing. **Seranthimata Samshuddin:** Data curation, Methodology, Writing – original draft.

Appendix A. Supplementary material

Supplementary data to this article can be found online at https://doi.org/10.1016/j.arabjc.2024.105752.

References

Abdelazim, K., Khaled, K., Abdelshafy, N., 2021. Studies on the Effect of Some Pyrimidine Derivatives on the Corrosion of Iron in 1M Hydrochloric Acid. Egypt. J. Chem. 64 (7), 3475–3488.

Ahmed, M.H., Othman, A.A., Al-Amiery, Y.K., Al-Majedy, A.A., Kadhum, H., Mohamad, A.B., Gaaz, T.S., 2018. Synthesis and characterization of a novel organic corrosion inhibitor for mild steel in 1 M hydrochloric acid. Results Phys. 8, 728–733.

Akinbulumo, O.A., Odejobi, O.J., Odekanle, E.L., 2020. Thermodynamics and adsorption study of the corrosion inhibition of mild steel by *Euphorbia heterophylla* L. extract in 1.5 M HCl. Results Mater. 5, 100074.

Al-Amiery, A.A., Abdul Amir, H., Kadhum, A.H., Alobaidy, M., Mohamad, A.B., Hoon, P. S., 2014. Novel corrosion inhibitor for mild steel in HCl. Materials 7 (2), 662–672.

Ammal, P.R., Prajila, M., Joseph, A., 2018. Effective inhibition of mild steel corrosion in hydrochloric acid using EBIMOT, a 1, 3, 4-oxadiazole derivative bearing a 2-ethyl-benzimidazole moiety: electro analytical, computational and kinetic studies, Egypt. J. Pet. 27 (4), 823–833.

Arrousse, N., Salim, R., Kaddouri, Y., Zarrouk, A., Zahri, D., Hajjaji, F.E., Touzani, R., Taleb, M., Jodeh, S., 2020. The inhibition behavior of two pyrimidine-pyrazole derivatives against corrosion in hydrochloric solution: Experimental, surface analysis and in silico approach studies. Arab. J. Chem. 13, 5949–5965.

Assad, H., Kumar, S., Saha, S.K., Kang, N., Fatma, I., Dahiya, H., Sharma, P.K., Thakur, A., Sharma, S., Ganjoo, R., Kumar, A., 2023. Evaluating the adsorption and corrosion inhibition capabilities of Pyridinium - P - Toluene sulphonate on MS in 1 M HCl medium: an experimental and theoretical study. Inorg. Chem. Commun. 153, 110817.

Avdeev, Y.G., Kuznetsov, Y.I., 2021. Nitrogen-containing five-membered heterocyclic compounds as corrosion inhibitors for metals in solutions of mineral acids-an overview. Int. J. Corros. Scale Inhibit. 10 (2), 480–540.

Becke, A.D., 1992. Density-functional thermochemistry. I. The effect of the exchange-only gradient correction. J. Chem. Phys. 96 (3), 2155–2160.

Bigi, F., Carloni, S., Frullanti, B., Maggi, R., Sartori, G., 1999. A revision of the biginelli reaction under solid acid catalysis. solvent-free synthesis of dihydropyrimidines over montmorillonite KSF. Tetrahedron Lett. 40 (17), 3465–3468.

Chakravarthy, M.P., Mohana, K.N., 2014. Adsorption and corrosion inhibition characteristics of some nicotinamide derivatives on mild steel in hydrochloric acid solution. Int. Scholarly Res. Notices 2014.

Chauhan, D.S., Quraishi, M.A., Qurashi, A., 2021. Recent trends in environmentally sustainable sweet corrosion inhibitors. J. Mol. Liq. 326, 115117.

Ech-Chihbi, E., Nahlé, A., Salim, R., Benhiba, F., Moussaif, A., El-Hajjaji, F., Oudda, H., Guenbour, A., Taleb, M., Warad, I., 2020. Computational, MD simulation, SEM/EDX and Experimental studies for understanding adsorption of benzimidazole derivatives as corrosion inhibitors in 1.0 M HCl solution. J. Alloy. Compd. 844, 155842.

Elewady, G.Y., 2008. Pyrimidine Derivatives as Corrosion Inhibitors for Carbon-Steel in 2M Hydrochloric Acid Solution. Int. J. Electrochem. Sci. 3, 1149–1161.

Elmsellem, H., Aouniti, A., Khoutoul, M.A., et al., 2014. Theoretical approach to the corrosion inhibition efficiency of some pyrimidine derivatives using DFT method of mild steel in HCl solution. J. Chem. Pharm. Res. 6, 1216–1224.

Ferigita, K.S., Miled, M.G., AlFalah, K., Saracoglu, M., Kokbudak, Z., Kaya, S., Alaghani, M.O.A., Kandemirli, F., 2022. Corrosion behaviour of new oxo-pyrimidine derivatives on mild steel in acidic media: experimental, surface characterization, theoretical, and Monte Carlo studies. Appl. Surface Sci. Adv. 7, 100200.

Ferigita, K.S.M., Saracoglu, M., AlFalah, M.G.K., Yilmazer, M.I., Kokbudak, Z., Kaya, S., Kandemirli, F., 2023. Corrosion inhibition of mild steel in acidic media using new oxo-pyrimidine derivatives: experimental and theoretical insights. J. Mol. Struct. 1284, 135361 https://doi.org/10.1016/j.molstruc.2023.135361.

Fytianos, G., Ucar, S., Grimstvedt, A., Svendsen, H.F., Knuutila, H., 2016. Corrosion evaluation of MEA solutions by SEM-EDS, ICP-MS and XRD. Energy Procedia 86, 197–204.

Guo, L., Kaya, S., Obot, I.B., Zheng, X., Qiang, Y., 2017. Toward understanding the anticorrosive mechanism of some Thiourea derivatives for carbon steel corrosion: a combined DFT and molecular dynamics investigation. J. Colloid Interface Sci. 506, 478–485.

Idris, Mohd Nazri, Abdul Razak Daud, and Norinsan Kamil Othman. 2013. "Electrochemical Impedance Spectroscopy Study on Corrosion Inhibition of Benzyltriethylammonium Chloride." In , 1571:23–28. American Institute of Physics.

Junaedi, Sutiana, Ahmed A Al-Amiery, Abdulhadi Kadihum, Abdul Amir H Kadhum, Abu Bakar Mohamad, 2013. Inhibition effects of a synthesized novel 4-aminoantipyrine derivative on the corrosion of mild steel in hydrochloric acid solution together with quantum chemical studies. Int. J. Mol. Sci. 14 (6): 11915–28.

Koch, G., 2017. Cost of corrosion. Trends Oil Gas Corros. Res. Technol. 3–30.

Kuş, E., Mansfeld, F., 2006. An evaluation of the electrochemical frequency modulation (EFM) technique. Corros. Sci. 48 (4), 965–979.

Lahmidi, S., Elyoussfi, A., Dafali, A., et al., 2017. Corrosion inhibition of mild steel by two new 1,2,4-triazolo[1,5-a] pyrimidine derivatives in 1 M HCl: Experimental and computational study. J. Mat. Env. Sci. 8, 225–237.

Lai, C., Xie, B., Zou, L., Zheng, X., Ma, X., Zhu, S., 2017. Adsorption and corrosion inhibition of mild steel in hydrochloric acid solution by S-allyl-O, O′-dialkyldithiophosphates. Results Phys. 7, 3434–3443.

Obot, I.B., Onyeachu, I.B., Umoren, S.A., 2018. Pyrazines as potential corrosion inhibitors for industrial metals and alloys: a review. J. Bio-and Tribo-Corrosi. 4, 1–13.

Obot, I.B., Meroufel, A., Onyeachu, I.B., Alenazi, A., Sorour, A.A., 2019a. Corrosion inhibitors for acid cleaning of desalination heat exchangers: progress, challenges and future perspectives. J. Mol. Liq. 296, 111760.

Obot, I.B., Solomon, M.M., Umoren, S.A., Suleiman, R., Elanany, M., Alanazi, N.M., Sorour, A.A., 2019b. Progress in the development of sour corrosion inhibitors: past, present, and future perspectives. J. Ind. Eng. Chem. 79, 1–18.

Obot, I.B., Onyeachu, I.B., Umoren, S.A., Quraishi, M.A., Sorour, A.A., Chen, T., Aljeaban, N., Wang, Q., 2020. High temperature sweet corrosion and inhibition in the oil and gas industry: progress, challenges and future perspectives. J. Pet. Sci. Eng. 185, 106469.

Oguike, R.S., Kolo, A.M., Shibdawa, A.M., Gyenna, H.A., 2013. Density functional theory of mild steel corrosion in acidic media using dyes as inhibitor: adsorption onto Fe (110) from gas phase. ISRN Physical Chemistry 2013, 1–9.

Onyeachu, I.B., Quraishi, M.A., Obot, I.B., Haque, J., 2019. Newly synthesized pyrimidine compound as CO2 corrosion inhibitor for steel in highly aggressive simulated oilfield brine. J. Adhes. Sci. Technol. 33 (11), 1226–1247.

Onyeachu, I.B., Quraishi, M.A., Obot, I.B., 2023a. A synthesized pyrimidine derivative with highly efficient long-term corrosion protection for API X60 steel in CO2-saturated NACE brine ID196 under hydrodynamic condition. J. Mol. Struct. 1284, 135399.

Onyeachu, I.B., Quraishi, M.A., Obot, I.B., 2023b. A synthesized pyrimidine derivative with highly efficient long-term corrosion protection for API X60 steel in CO2-saturated NACE brine ID196 under hydrodynamic condition. J. Mol. Struct. 1284 (July), 135399 https://doi.org/10.1016/j.molstruc.2023.135399.

Ouakki, M., Galai, M., Cherkaoui, M., 2022. Imidazole derivatives as efficient and potential class of corrosion inhibitors for metals and alloys in aqueous electrolytes: a review. J. Mol. Liq. 345, 117815.

Paul, P.K., Yadav, M., 2020. Investigation on corrosion inhibition and adsorption mechanism of triazine-thiourea derivatives at mild Steel/HCl solution interface: electrochemical, XPS, DFT and Monte Carlo simulation approach. J. Electroanal. Chem. 877, 114599.

Praveen, B.M., Alhadhrami, A., Prasanna, B.M., Hebbar, N., Prabhu, R., 2021. Anti-corrosion behavior of olmesartan for soft-cast steel in 1 Mol Dm− 3 HCl. Coatings 11 (8), 965.

Rasheeda, K., Alamri, A.H., Krishnaprasad, P.A., Phadke Swathi, N., Alva, V.DP., Aljohani, T.A., 2022a. Efficiency of a pyrimidine derivative for the corrosion inhibition of C1018 Carbon steel in aqueous acidic medium: Experimental and theoretical approach. Colloids Surf A Physicochem Eng Asp 642, 128631.

Rasheeda, K., Phadke Swathi, N., Alva, V.DP., Aljohani, T.A., Alomari, F.Y., Alamri, A.H., 2022b. Anticorrosive behavior of new pyrimidine derivatives on Carbon steel in acidic medium: experimental, theoretical, and Surface studies. Journal of Bio-and Tribo-Corrosion 8 (4), 89.

Rehim, Sayed S Abdel, Omar A Hazzazi, Mohammed A Amin, and Khaled F Khaled. 2008. "On the Corrosion Inhibition of Low Carbon Steel in Concentrated Sulphuric Acid Solutions. Part I: Chemical and Electrochemical (AC and DC) Studies." *Corrosion Science* 50 (8): 2258–71.

Saadouni, M., Galai, M., Aoufir Yel Skal, S., Boukhris, S., Hassikou, A., Touhami, M.E., Guenbour, A., El Khlifi, A., Oudda, H., Habbadi, N., 2018. Experimental and quantum chemical and Monte Carlo simulations studies on the corrosion inhibition of mild steel in 1 M HCl by two benzothiazine derivatives. J. Mater. Environ. Sci. 9, 2493–2504.

Sliem, M.H., El Basiony, N.M., Zaki, E.G., Sharaf, M.A., Abdullah, A.M., 2020. Corrosion inhibition of mild steel in sulfuric acid by a newly synthesized Schiff Base: an electrochemical, DFT, and Monte Carlo simulation study. Electroanalysis 32 (12), 3145–3158.

Sun, H., 1998. COMPASS: an ab initio force-field optimized for condensed-phase applications overview with details on alkane and benzene compounds. J. Phys. Chem. B 102 (38), 7338–7364.

Swathi, N.P., Samshuddin, S., Aljohani, T.A., Rasheeda, K., Alva, V.D.P., Baig, I., Maslamani, N., Hassan Alamri, A., 2023. Investigation of some new triazole derivatives for inhibiting the acid corrosion of C1018 carbon steel: correlation of electrochemical studies with quantum chemical calculations. S. Afr. J. Chem. Eng. 44, 123–134.

Tiongson, Julius Kim A, Kim Christopher C Aganda, Dwight Angelo V Bruzon, Albert P Guevara, Blessie A Basilia, Giovanni A Tapang, and Imee Su Martinez. 2020. Exploring the Corrosion Inhibition Capability of FAP-Based Ionic Liquids on Stainless Steel. Royal Society Open Science 7 (7): 200580.

Verma, C., Quraishi, M.A., Singh, A., 2015. 2-Amino-5-nitro-4, 6-diarylcyclohex-1-ene-1, 3, 3-tricarbonitriles as new and effective corrosion inhibitors for mild steel in 1 M HCl: experimental and theoretical studies. J. Mol. Liq. 212, 804–812.

Verma, C., Ebenso, E.E., Quraishi, M.A., Hussain, C.M., 2021. Recent developments in sustainable corrosion inhibitors: design, performance and industrial scale applications. Mater. Adv. 2 (12), 3806–3850.

Verma, C., Thakur, A., Ganjoo, R., Sharma, S., Assad, H., Kumar, A., Quraishi, M.A., Alfantazi, A., 2023. Coordination bonding and corrosion inhibition potential of nitrogen-rich heterocycles: azoles and triazines as specific examples. Coord. Chem. Rev. 488, 215177.

Yadav, M., Sharma, U., Yadav, P.N., 2013. Isatin compounds as corrosion inhibitors for N80 steel in 15% HCl. Egypt. J. Pet. 22 (3), 335–344.

Yadav, M., Kumar, S., Sinha, R.R., Bahadur, I., Ebenso, E.E., 2015. New pyrimidine derivatives as efficient organic inhibitors on mild steel corrosion in acidic medium: Electrochemical, SEM, EDX, AFM and DFT studies. J. Mol. Liq. 211, 135–145.

Yadav, M., Sarkar, T.K., Purkait, T., 2015a. Amino acid compounds as eco-friendly corrosion inhibitor for N80 steel in HCl solution: electrochemical and theoretical approaches. J. Mol. Liq. 212, 731–778.
Yadav, M., Sinha, R.R., Sarkar, T.K., Bahadur, I., Ebenso, E.E., 2015b. Application of new isonicotinamides as a corrosion inhibitor on mild steel in acidic medium: electrochemical, SEM, EDX, AFM and DFT investigations. J. Mol. Liq. 212, 686–698.
Yüce, A.O., Mert, B.D., Kardaş, G., Yazıcı, B., 2014. Electrochemical and quantum chemical studies of 2-amino-4-methyl-thiazole as corrosion inhibitor for mild steel in HCl solution. Corros. Sci. 83, 310–336.